Virtually Imaged Phase Array (VIPA)-Based Wavelength Selective Switch with High Spectral Resolution

Haoshuo Chen(1), Nicolas K. Fontaine(1), Mikael Mazur(1), Roland Ryf(1), and David T. Neilson(1)

(1) Nokia Bell Labs, 791 Holmdel Rd., Holmdel, New Jersey 07733, USA
haoshuo.chen@nokia-bell-labs.com

Abstract *We present a 10-port VIPA-based WSS with 3-GHz spectral resolution. A new attenuation scheme through destructively interfering different diffraction orders from the VIPA is proposed and experimentally demonstrated.*

Introduction

Driven by the need for virtual conferencing, video streaming and Cloud services, we continue to observe rapid network traffic growth over the years[1]. In order to continue to increase the capacity of optical communication systems, spatial parallelism employing multiple spatial modes[2], ultra-broadband transmission exploring new optical wavelength bands[3] and ultra-high spectral efficiency schemes using high-order quadrature and in-phase modulation (QAM) and probabilistic shaping[4] are being explored. To support flexible optical networking, wavelength selective switches (WSS) supporting space-division multiplexing of fibers and new wavelength bands such as S-band have been successfully demonstrated[5],[6]. However, the resolution of most diffraction grating based WSS is larger than 10 GHz, which makes it challenging to closely pack the high-order QAM signals which are currently operated at lower sample rates to avoid performance degradation at high frequency[4],[7]. Achieving higher spectral resolution requires devices with larger angular dispersion such as virtually imaged phase array (VIPA) which has enabled high resolution wavelength demultiplexers and pulse shapers[8],[9].

In this paper, we propose to use a VIPA as the spectral disperser to enhance the spectral resolution of WSS. We experimentally demonstrate a 10-port VIPA-based WSS which obtains a 3-GHz 90%-to-10% transition resolution and can produce a flat-top passband on a 10-GHz grid. A novel channel attenuation scheme based on destructive interference by introducing phase difference between different diffraction orders of the VIPA is also demonstrated.

Enhanced Spectral Resolution

Conventional WSS designs use a diffraction grating to spectrally disperse the light. The minimum frequency difference $\Delta\nu$, with ν denoting the operation frequency, between two neighboring frequencies ν and $\nu + \Delta\nu$ that can be distinguished is then given by the Rayleigh criterion. The ratio $\nu/\Delta\nu$ is then given by $\nu/\Delta\nu = mNW$, where m is the diffracted order, N is the number of lines per mm and W is the width of the grating illuminated by the incoming beam. For a typical WSS grating with N of 1200 lines/mm, W of 10 mm and operating at 1^{st} order, the resolvable frequency difference $\Delta\nu$ is around 16 GHz at C-band.

In contrast, VIPA provides a much larger angular dispersion due to its Fabry-Perot etalon geometry[8],[10]. The VIPA used in this experiment is fabricated on fused silica. It has a thickness of 0.5 mm, a height of 24 mm (wavelength and order direction) and a width of 30 mm (port direction). Successive virtual sources are generated after the input beam is being reflected between the two surfaces of the VIPA , thereby forming a phase array. More than 400 virtual sources can be generated using this VIPA with optimum input beam waist and angle. The maximum path length difference is more than 0.4 m, which corresponds to 2-ns time delay in fused silica. The inverse of the time delay indicates that the VIPA spectral resolution can be as high as 0.5 GHz, which is more than one order of magnitude finer than can be achieved using a conventional diffraction grating. The free spectral range (FSR) of the VIPA is around 205 GHz determined by the path length difference between two neighboring virtual sources.

VIPA-Based WSS

Figure 1(a) illustrates the operating principle of the VIPA-based WSS. The picture of the built VIPA-based WSS supporting 10 ports is shown in Fig. 1(b), with an inset to show the VIPA. The WSS input consist of a 127 μm pitch fiber array

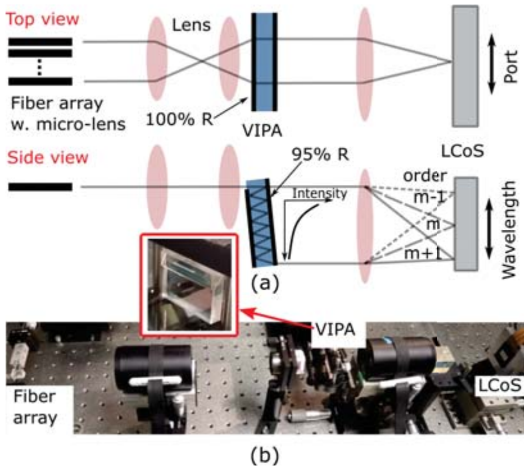

Fig. 1: (a) Illustration of the operating principle of the VIPA-based WSS: (upper) at port steering direction, in which a 2-f relay converts steering angle of the LCoS to a port position; (lower) at wavelength direction, where the system forms a 2-f relay after the VIPA to spatially disperse the light on the LCoS, (b) picture of the built VIPA-based WSS supporting 10 ports. The inset shows the VIPA with a thickness of 0.5 mm and height of 24 mm (R: reflectivity).

with microlenses to provide 10 collimated 36-μm waist beams. These are first demagnified by a factor of 2.8 using a 4-f relay consisting of two bulk circular lenses to achieve optimum beam waist in the wavelength direction before being directed into the input window of the VIPA. The input window has an anti-reflection coating and the remaining part of the back side coated for 100% reflectivity. The opposite side, facing the forward direction in the system, has a reflectivity of 95%. A circular spectrometer lens is then applied for angle-to-position conversion, which separates different wavelengths and orders vertically on a reflective Holoeye liquid crystal on silicon (LCoS) panel with 1920 $\times$ 1080 pixels and 8-μm pixel size. The long axis of the LCoS is used for port steering. As a proof-of-concept demonstration, polarization diversity is not implemented in this experiment, which can be achieved by either adding polarization diversity optics in the port direction[6] or using two LCoS panels to steer each polarization[11].

Mapping between the pixel number of the LCoS at wavelength direction (LCoS's short axis) and the frequency is characterized. Results measured at the center along the LCoS's long axis are plotted in Fig 2(a). We choose one FSR from 193.9 to 194.005 THz as the calibration frequency range to have two orders with identical power intensity to realize attenuation using destructive interference. Intensity of all the modes follows a Gaussian-like distribution[9] as shown in Fig 2(b). Figure 2(c) provides the power distribution image at the LCoS plane for a continuous wave (CW)

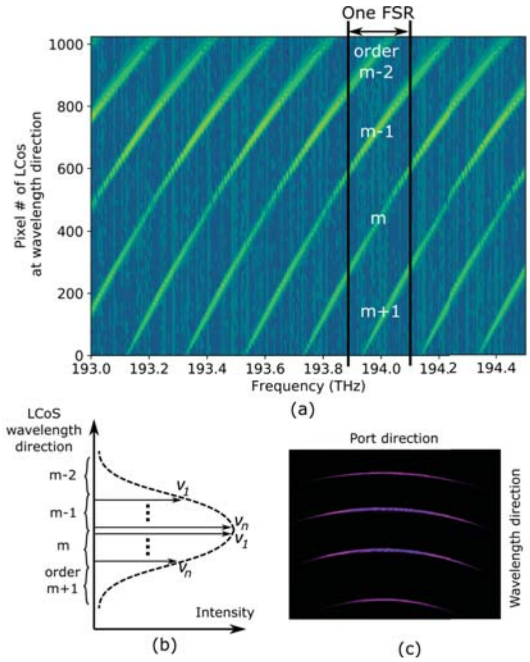

Fig. 2: (a) Measured mapping between the pixel number of the LCoS at wavelength direction and the frequency, (b) schematics of VIPA's output intensity envelope and chosen frequency range to have two diffraction orders with identical power intensity and (c) captured power distribution of a 194-THz CW light by a camera.

light at 194 THz captured by a camera. Since order $m-2$ and $m+1$ are only partially covered by the LCoS, they are not applied in steering. Dispersion characteristics for the two center orders are calibrated sequentially.

Experimental Results

The 10-port WSS is calibrated using spectral transmission measurements from a multi-port swept-wavelength interferometer. The minimum insertion loss (IL) of the WSS is around 9 dB. Virtual sources experience an exponential decay from the uniform 95$\%$ reflectivity, which makes the output beam profile of the VIPA asymmetric, see Fig 1(a). More than 4-dB loss is introduced by this asymmetry which reduces the field overlap between the forward and backward propagation light since the profile of the latter is inverted after passing the spectrometer lens twice. This loss can be mitigated using a VIPA with graded reflectivity which can produce a symmetric beam profile[10]. Moreover, the IL can be further reduced utilizing more diffraction orders.

Figure 3(a) shows the transmission from interleaving two ports on a 10-GHz grid, which has a repetitive pattern over each FSR. Zoomed-in transmission over one FSR is given in Fig. 3(b). Figure 3(c) shows the results of directing different frequency channels to different ports on a 10-GHz grid. Figure 3(d) shows the passbands un-

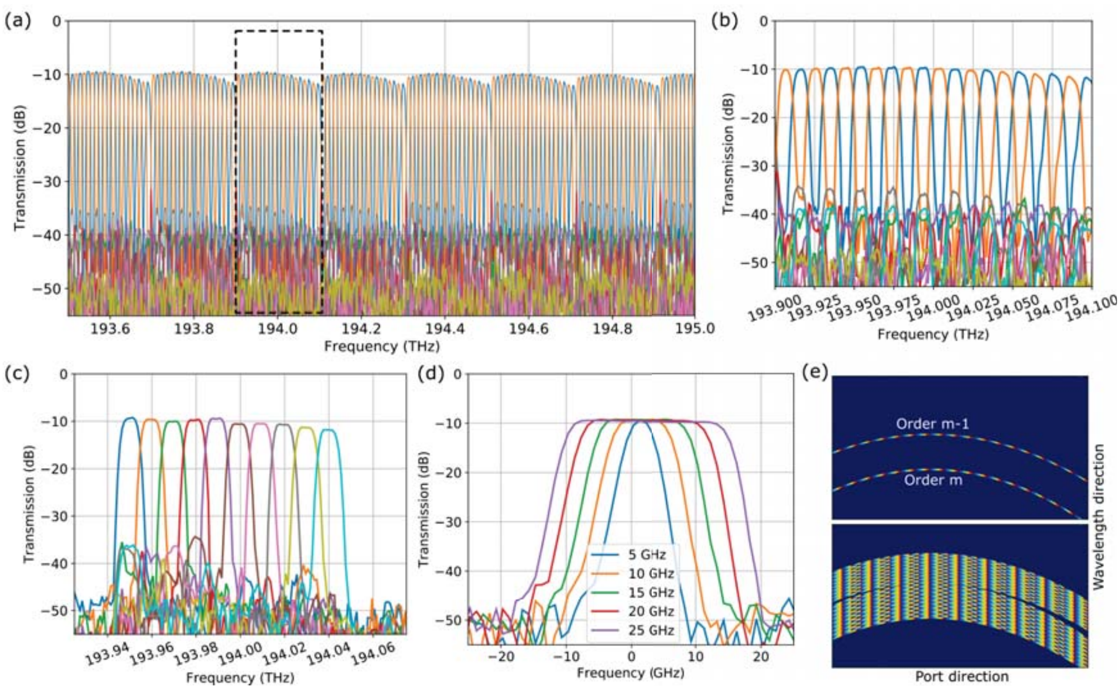

Fig. 3: (a) Interleaved pattern on a 10-GHz grid and (b) its zoomed feature over one FSR, (c) transmission for directing different channels to different ports on a 10-GHz grid, (d) transmission under different bandwidth settings and (e) hologram for (upper) switching a single 10-GHz channel and (lower) interleaved pattern of Fig. 3(a).

der different bandwidths. Spectral dispersion on the LCoS is around 0.7 GHz/pixel. Measured resolution is $<$ 3 GHz using a metric with 90% to 10% power transition at the passband edge[12]. This discrepancy can be attributed to the LCoS's pixel crosstalk and the exponential decay from the VIPA which weakens the contributions from the virtual sources with larger delays. The resolution can be improved using a LCoS panel with a smaller pixel-to-pixel crosstalk and a VIPA with graded reflectivity. Hologram examples projected on the LCoS are shown in Fig. 3(e).

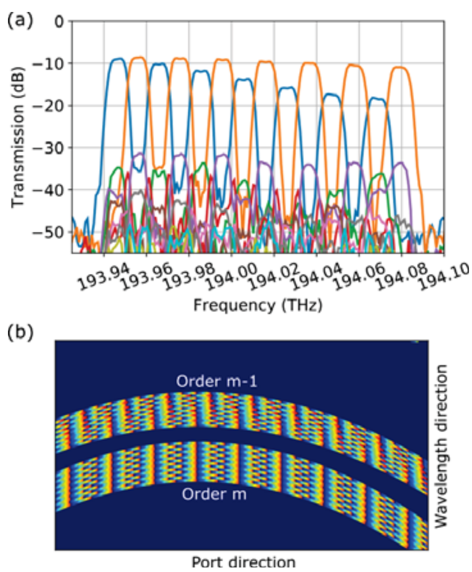

Fig. 4: (a) Interleaved pattern on a 10-GHz grid with odd channels experiencing a gradual 1.5-dB attenuation and (b) hologram applied for the attenuation.

Attenuation in WSS is usually accomplished through complex holograms that throw away the attenuated light to spatial frequencies far from the ports. This reduces the maximum number of ports because some are dummy ports used for attenuation and requires additional efforts to optimize the holograms for low crosstalk. Leveraging the diffraction orders, channel attenuation through destructive interference can be accomplished after phase shifting one order to introduce phase difference. This attenuation scheme can fully isolate attenuation from port steering, which is beneficial in crosstalk reduction and avoiding delicate hologram optimization needed in conventional WSS. Figure 4(a) shows the interleaved pattern on a 10-GHz grid as odd channels are attenuated gradually with a 1.5-dB increment. The hologram applied for the attenuation is provided in Fig 4(b). Besides attenuation, power splitting can also be realized by directing different orders to different ports without using troublesome splitting holograms[11].

Conclusions

We experimentally demonstrated a 10-port VIPA-based WSS with a high spectral resolution around 3 GHz and 205-GHz FSR. Utilizing multiple diffraction orders from the VIPA enables the functionalities such as attenuation and power splitting without requiring sophisticated hologram optimization.

References

[1] P. J. Winzer and D. T. Neilson, "From Scaling Disparities to Integrated Parallelism: A Decathlon for a Decade", *J. Lightwave Technol.*, vol. 35, no. 5, pp. 1099–1115, Mar. 2017.

[2] G. Rademacher, R. S. Luis, B. Puttnam, R. Ryf, S. Van Der Heide, T. A. Eriksson, N. K. Fontaine, H. Chen, R.-J. Essiambre, Y. Awaji, H. Furukawa, and N. Wada, "High Capacity Transmission in a Coupled-Core Three-Core Multi-Core Fiber", *Journal of Lightwave Technology*, pp. 1–1, 2020.

[3] A. Arnould, A. Ghazisaeidi, D. L. Gac, P. Brindel, M. Makhsiyan, K. Mekhazni, F. Blache, N. Fontaine, D. Neilson, R. Ryf, H. Chen, M. Achouche, and J. Renaudier, "103 nm Ultra-Wideband Hybrid Raman/SOA Transmission Over 3 x 100 km SSMF", *J. Lightwave Technol., JLT*, vol. 38, no. 2, pp. 504–508, Jan. 2020.

[4] S. L. Olsson, J. Cho, S. Chandrasekhar, X. Chen, P. J. Winzer, and S. Makovejs, "Probabilistically shaped PDM 4096-QAM transmission over up to 200 km of fiber using standard intradyne detection", *Opt. Express*, vol. 26, no. 4, p. 4522, Feb. 2018.

[5] D. M. Marom, P. D. Colbourne, A. Dâerrico, N. K. Fontaine, Y. Ikuma, R. Proietti, L. Zong, J. M. Rivas-Moscoso, and I. Tomkos, "Survey of photonic switching architectures and technologies in support of spatially and spectrally flexible optical networking [invited]", *IEEE/OSA Journal of Optical Communications and Networking*, vol. 9, no. 1, pp. 1–26, Jan. 2017.

[6] N. K. Fontaine, R. Ryf, D. T. Neilson, and H. Chen, "Low Loss Wavelength Selective Switch with 15-THz Bandwidth", in *2018 European Conference on Optical Communication (ECOC)*, Rome, Sep. 2018, pp. 1–3.

[7] M. Terayama, S. Okamoto, K. Kasai, M. Yoshida, and M. Nakazawa, "4096 QAM (72 Gbit/s) Single-Carrier Coherent Optical Transmission with a Potential SE of 15.8 bit/s/Hz in All-Raman Amplified 160 km Fiber Link", in *2018 Optical Fiber Communications Conference and Exposition (OFC)*, Mar. 2018, pp. 1–3.

[8] M. Shirasaki, "Large angular dispersion by a virtually imaged phased array and its application to a wavelength demultiplexer", *Opt. Lett.*, vol. 21, no. 5, p. 366, Mar. 1996.

[9] V. R. Supradeepa, E. Hamidi, D. E. Leaird, and A. M. Weiner, "New aspects of temporal dispersion in high-resolution Fourier pulse shaping: A quantitative description with virtually imaged phased array pulse shapers", *J. Opt. Soc. Am. B, JOSAB*, vol. 27, no. 9, pp. 1833–1844, Sep. 2010.

[10] M. Shirasaki, A. Akhter, and C. Lin, "Virtually imaged phased array with graded reflectivity", *IEEE Photonics Technology Letters*, vol. 11, no. 11, pp. 1443–1445, Nov. 1999.

[11] H. Chen, N. K. Fontaine, R. Ryf, and D. T. Neilson, "LCoS-Based Photonic Crossconnect", in *Optical Fiber Communication Conference (OFC) 2019*, San Diego, California, 2019, Th1E.6.

[12] N. Goldshtein, D. Sinefeld, O. Ori, L. Pascar, L. Pascar, R. Zektzer, and D. M. Marom, "Fine Resolution Photonic Spectral Processor Using a Waveguide Grating Router With Permanent Phase Trimming", *J. Lightwave Technol.*, vol. 34, no. 2, pp. 379–385, Jan. 2016.